THEORETICAL MODELLING AND SIMULATION OF PRISTINE LFP AND Ni DOPED LFP AS CATHODE MATERIAL OF LITHIUM ION BATTERY

A DISSERTATION

SUBMITTED IN PARTIAL FULFILLMENT OF THE REQUIREMENTS
FOR THE AWARD OF DEGREE
OF

MASTER OF TECHNOLOGY

IN

NANOSCIENCE AND TECHNOLOGY

Submitted By

SACHIN KHARB

(Roll No. 2K17/NST/03)

Under the supervision of

Dr. AMRISH K. PANWAR

(Assistant Professor)

DEPARTMENT OF APPLIED PHYSICS

Delhi Technological University

(Formerly Delhi College of Engineering)

Bawana Road, Delhi-110042

JULY 2019

DELHI TECHNOLOGICAL UNIVERSITY

(Formerly Delhi College of Engineering)

Bawana Road, Delhi-110042

CANDIDATE'S DECLARATION

I, SACHIN KHARB, Roll No. 2K17/NST/03 of M.Tech. Nanoscience and Technology, hereby declare that the project Dissertation titled **"Theoretical Modelling And Simulation Of Pristine LFP And Ni Doped LFP As Cathode Material Of Lithium Ion Battery"** which is submitted by me to the Department of Applied Physics, Delhi Technological University, Delhi in partial fulfillment of the requirement for the award of the degree of Master of technology, is original and not copied from any source without proper citation. This work has not previously formed the basis for the award of any Degree, Diploma Associateship, Fellowship or other similar title or recognition.

Place, Delhi, INDIA

Date:

Sachin Kharb

M.Tech (NST), DTU

Roll NO. 2K17/NST/03

DELHI TECHNOLOGICAL UNIVERSITY

(Formerly Delhi College of Engineering)

Bawana Road, Delhi-110042

CERTIFICATE

I hereby certify that the Project Dissertation titled **"Theoretical Modelling And Simulation Of Pristine LFP And Ni Doped LFP As Cathode Material Of Lithium Ion Battery"** by **Sachin Kharb**, Roll No. **2K17/NST/03**, Department of Applied Physics, Delhi in partial fulfillment of the requirement for the award of the degree of Master of Technology, is a record of the project work carried out by the student under my supervision. To the best of my knowledge, this work has not been submitted or full for any Degree or Diploma to this University or elsewhere.

Dr Amrish K Panwar
Assistant Professor
Delhi Technological University
Delhi, INDIA

Prof. Rinku Sharma
HOD, Applied Physics
Delhi Technological University
Delhi, INDIA

ACKNOWLEDGEMENT

With great pleasure I would like to express my first and sincere gratitude to my supervisor Dr. Amrish K. Panwar for his continuous support, patience, motivating ideas, enthusiasm and immense knowledge. His guidance has always enlightened and helped me to shape and develop my work.

Besides my supervisor, I would like to express my deep gratitude and respect to Prof. Rinku Sharma, Head, Department of Applied Physics, Delhi Technological University, Delhi, for her encouragement, insightful comments and valuable suggestion during the course. I would also like to thank Dr. M.S. Mehata , M.Tech coordinator and Assistant Professor, for his constant support and guidance throughout my studies.

I wish to extend my thanks to Mr. Abhishek Bhardwaj, Mr. Anurag Kaushik, Ms. Anchali Jain, Ms. Snigdha Sharma and Ms. Shivangi Rajput for their help, cooperation, advice and assistance in keeping my progress on schedule. I am highly obliged for their valuable and constructive suggestions during the planning and development of this research work.

I would also like to thank my friends Supriya Biswas and Jyotsana for keeping me motivated throughout the project working and development, and a special thanks to my seniors and friends Anurag and Sagar Khanna.

Contents

List of Figures

List of Tables

List of Equations

ABSTRACT

A simulation model for electrochemical impedance spectroscopy (EIS) of pristine $LiFePO_4$ (LFP), doped with various concentrations of Ni such as $LiNi_{.03}Fe_{0.97}PO_4$ (LFNP3), $LiNi_{.05}Fe_{0.95}PO_4$ (LFNP5) and $LiNi_{.07}Fe_{0.93}PO_4$ (LFNP7) in place of Fe has been developed in COMSOL Multiphysics. The model was studied under constant frequency domain perturbation using AC current impulses of 5-10 mA in frequency range 10kHz-10mHz. The simulated model parameters, which depict ideal conditions were varied one at a time, and then, two at a time to bring them close to experimental performance as extracted from experimental data.

Among all the undoped and Ni doped LFP samples, lithium iron phosphate doped with 3% Ni i.e. $LiNi_{.03}Fe_{0.97}PO_4$ comes close to 92% of the theoretical predicted yield [55], which translates to a maximum electrode state of charge of 0.9-0.92.

The dielectric constant of pristine LFP, LFNP3, LFNP5 and LFNP7 is dependent on frequency of operation and affects the capacitance of electrode as the frequency domain perturbation is investigated.

At low level of doping, the electrochemical performance improves, but on increasing the doping content of Ni more than 5 %, the resistances increase beyond that of pristine LPF.

Chapter 1

Introduction

1.1 Background

Energy has a central role in all human activities. Despite the advancements in energy generation, the energy sector is still struggling to get a robust, high density, portable and scalable solution for energy storage in required form factors, from small scale like smart watches to big scale such as cars/ hybrid electric vehicle. The energy consumption has gone up dramatically in past few decades as shown in figures 1.1 and 1.2 below:

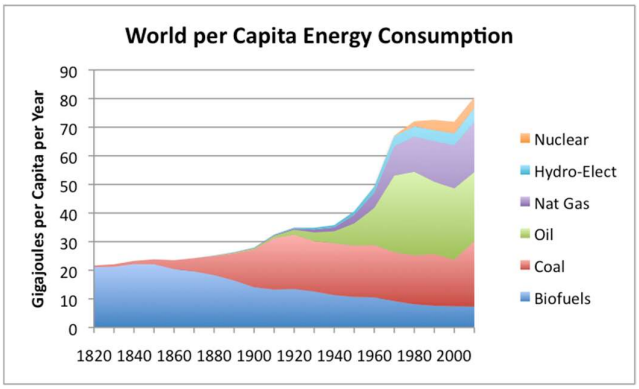

Fig 1.1 World Energy Consumption by Source[1],

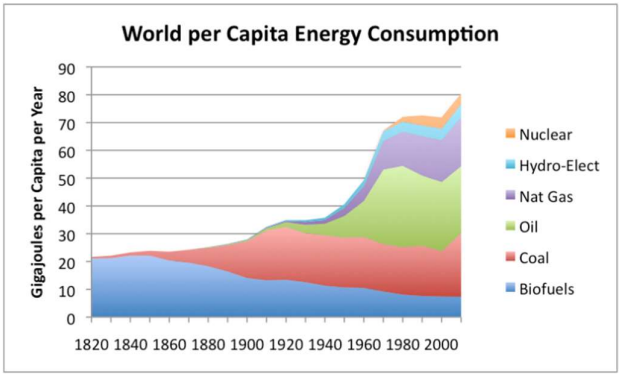

Fig 1.2. Per capita world energy consumption [1]

1.2 Battery

A battery is a collection of cell or cell assemblies and, cell is an electrochemical unit which comprises of a negative electrode, a positive electrode, a separator, and an electrolyte. Electricity is said to be generated due to a series of chemical reactions which take place because of involvement of chemical species of the electrodes and electrolyte. Thus, "any device which is capable of generating electrical energy by transforming chemical energy can be defined as a battery". When an external load is connected, the electrons move from the negative terminal in the direction of the positive terminal, which results in generation of an electric current. This current can be used to power a light bulb, computer, electric vehicles, clocks, mobile phones, and several other electronic devices [2]. A battery is unable to produce electricity if the electrode material is consumed completely as the separated charges may no more be available. As a result only, a limited amount of power may be available in the battery. However, a lot of batteries can be refurbished by altering the course of flow of electrons by means of a different source of power, these are known as rechargeable batteries. The reversal of electrochemical processes inside the battery, restore the positive and the negative electrode to their original state and the battery can be used again, this process is called charging.

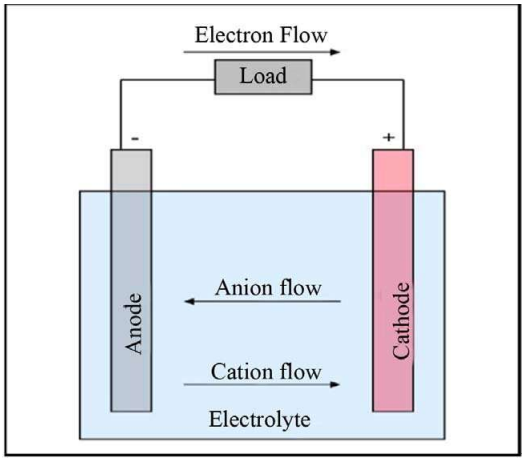

Figure 1.3 Working principle of a Battery [2]

1.2.1 History of Rechargeable Batteries

In 1859, Gaston Planté, conceived the idea of the first rechargeable (aka secondary) battery. The first lead acid cell prototype included sulfuric acid and a reel of two sheets of lead. Passage of reverse current through it results in the restoration of the reaction mechanism. Camille Alphonso Faure improved the design in 1881 by replacing the spiral sheet with plates. A plate was formed by devising a network of lead, embedded with lead oxide. This resulted in a scalable production chain and wide-spread use into automobile industry [4].

In 1970's, Nickel-hydrogen battery were developed by "COMSAT for communication satellites". Nickel-metal hydride (NiMH) batteries came into existence in the later years. The rechargeable batteries being an affordable and smaller alternative to nickel-hydrogen cells were very well received by consumers. In 1912, G.N. Lewis experimented with Lithium batteries and they struck the market in 1970. The first Lithium-ion battery was developed by Asahi Chemical of Japan. Lithium ion battery is rechargeable and is more stable adaptation of Lithium battery. In 1991, commercialization of the first Lithium-ion battery was done by Sony [6]. Lithium polymer battery were introduced in 1997, which stored the electrolyte in a solid polymer composite [5].

Fig 1.4 A lithium ion rechargeable battery [5]

1.3 Lithium-ion Battery

Being the lightest metal in the periodic table, Lithium possesses highest electrochemical potential and delivers largest specific energy per weight. "Although using Lithium metal as an anode in the rechargeable batteries provided extraordinarily high energy densities, unwanted dendrites growth on anode during cycling became a major issue with such batteries, as it resulted into electrical short." With the volatility of metallic lithium, the research studies provided a solution using "Lithium-ion". When Sony commercialized the first "Lithium-ion battery" in 1991, "Lithium-ion battery" became the fastest growing battery in the industry.

Lithium-ion battery are most commonly used in consumer and home electronics. Even though their specific energy is lower than the Lithium-metal, they are significantly safer when used within the specified limits of voltage and current ratings. Over the years, the reduced manufacturing cost, increased specific energy and, the absence of toxic elements has made Li-ion the most desirable rechargeable battery for portable applications, satellite application, heavy industries and electric vehicles. Also, when paralleled to other batteries under same category, such as nickel-cadmium or nickel-metal hydride, "Lithium-ion batteries don't suffer from memory effect, show minimal self-discharge (5-10°0) and, have very high energy density." Lithium-ion batteries possess a theoretical voltage of 4.1 V and practical voltage of 3.7 V with a longer life period (10004-cycles) compared to nickel-cadmium (1.2 V, 500 cycles) and nickel-metal hydride (1.4 V, 600 cycles) [5].

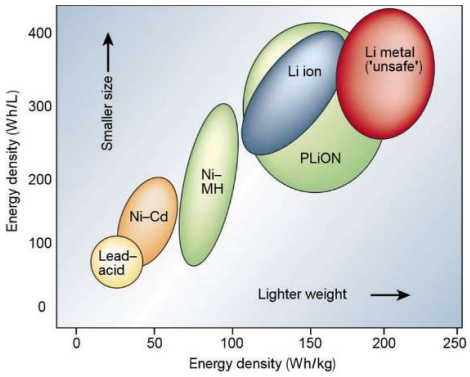

Fig 1.5: Energy Density of various battery types. [5]

1.3.1. History of Lithium-ion Battery

Research to develop the batteries which used lithium compounds in place of lithium, for safety concerns, began. In 1974-76, Besenhard, discovered and proposed "the application of reversible intercalation in graphite and intercalation in cathodic oxides". Samar Basu's experiment demonstrating intercalation of lithium in graphite, resulted in development of LiC_6 electrode at Bell labs in 1977. In 1979, John B. Goodenough invented the Lithium-cobalt-oxide battery. "This battery used $LiCoO_2$ as the positive electrode and lithium metal as the negative electrode." This laid the foundation to the prospects of using stable and efficient materials as negative electrodes instead of Lithium-metal. A variety of ternary compounds, such as $LiMnO_4$, $LiMnO_3$, Lithium-Copper-oxide and Lithium-nickel-oxide, were also identified along with lithium-cobalt-oxide in the later years. Rashid Yazami explained the reversible lithiation in graphite using a solid electrolyte. These graphite electrodes discovered by "Yazami" are the universally accepted electrodes used in Li-ion batteries. In 1983, "John. B. Goodenough et al" exploited manganese spinel as a promising positive electrode for lithium-ion batteries. The use of spinel electrodes in commercial batteries started from the year 2013. The prototype cell using $LiCoO_2$ as the positive electrode and a carbon rich material in which lithium ions could be fitted was assembled in 1985. John Goodenough also established that higher voltages could be achieved when poly-

anions such as sulfates are used as the positive electrodes. "The first commercial Lithium-ion battery was introduced by Sony and Asahi Kasei in 1991"[6]. Over the years, $LiFePO_4$, lithium-metal phosphates (olivine), lithium-nickel-manganese-cobalt-oxide and several other materials were recognized to be successfully implemented as positive electrodes. In recent years, graphite as the anode material has also been replaced by silicon, Lithium-titanate (LTO), tin/cobalt alloys etc. There are several ongoing researches to find low voltage anode materials without compromising the energy stored per unit volume. "The current global lithium-ion battery production capacity is marked at 28 GWh" [7-11].

1.3.2. Construction of a Lithium-ion battery

Like any standard battery, a lithium-ion battery is also composed of a positive electrode, a negative electrode, electrolyte, separators and casings. The positive electrode in a conventional lithium-ion battery is a metal-oxide such as $LiCoO_2$ or $LiFePO_4$. The negative electrode consists of porous carbon (commonly graphite) and the electrolyte is a lithium salt dissolved in organic solvent (usually 1:2 EC:DMC : $LiPF_6$). The electrochemical characteristics of the electrodes reverse between the anode and the cathode conditional to the current direction. The separator used is usually a micro perforated sheet of plastic which prevents the positive and the negative electrodes to come in contact and allows ions to pass through it. The outer case is made of metal which comes with a pressure sensitive vent because of the pressurized battery [13-14].

1.3.3. Electrochemistry

Lithium-ions move in and out of the electrodes through the process called intercalation/insertion (lithiation) and de-intercalation/extraction (de-lithiation). "When the battery undergoes charging, the positively charged lithium ions move from the positive electrode towards the negative electrode through the electrolyte while the electrons move in the same direction via an external circuit". Implantation of these lithium ions in the negative electrode occurs by a process known as lithiation or intercalation. While discharging, oxidation at the negative electrode occurs and the electrons and lithium-ions move towards the positive electrode via an external circuit and electrolyte, respectively. This process of removal of lithium ions is known as de-intercalation. While discharging, oxidation, defined as the electrons loss, occurs at the negative terminal while reduction which may be defined as electron benefit occurs at the positive terminal. This passage of positive ions from anode to the cathode causes a current to flow within the circuit. Similarly, charging results in oxidation at the positive terminal and reduction at the negative terminal and the applied overvoltage induces a charging current within the circuit [15-17].

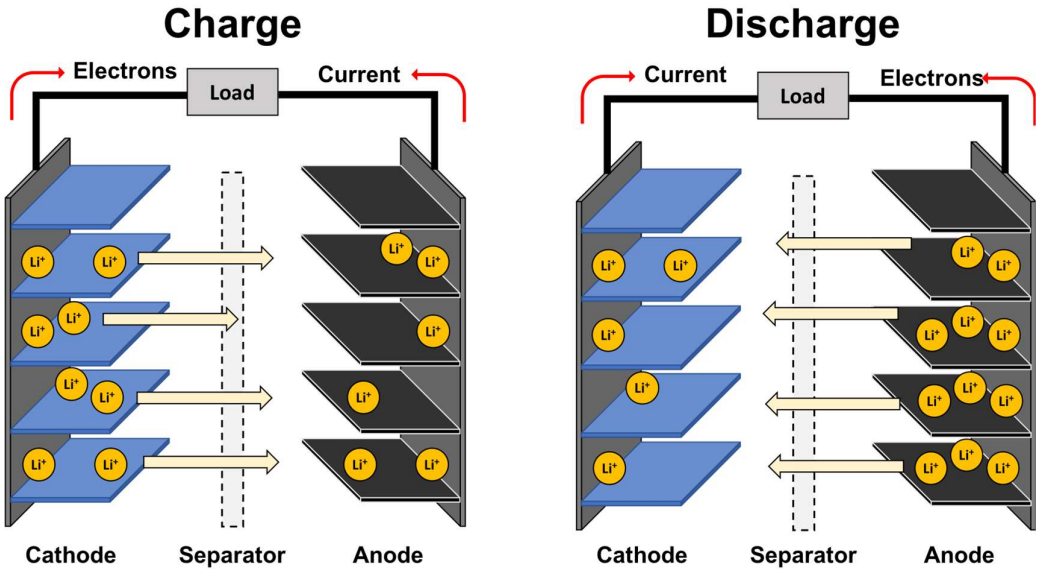

Fig 1.6. Ion flow in lithium-ion battery while charging and discharging. [18]

At positive electrode, the reaction which occurs is:

$$CoO_2 + Li^+ + e^- = LiCoO_2 \quad (1.1)$$

And at the negative electrode:

$$LiC_6 \rightleftharpoons C_6 + Li^+ + e^- \quad (1.2)$$

The overall reaction occurring in a Lithium-ion battery

$$LiC_6 + CoO_2 \rightleftharpoons C_6 + LiCoO_2 \quad (1.3)$$

Even with excellent rechargeable properties, lithium-ion batteries suffer from various losses during the first intercalation/de-intercalation process. Formation of resistive film around particles during the first charging and discharging is considered to be one of the major losses that occurs in the Li-ion batteries. This SEI coating forms due to "interaction between the electrode materials and the electrolyte". It provides electrical insulation, and increased ionic conductivity and also prevents intercalation of solvent into the electrode. Lithium-oxide, lithium-fluoride, and semi-carbonates together constitute the SEI.

1.3.4. Electrode materials

The materials that fulfil the criteria of having good electrical conductivity, decent ionic conductivity, reversible capacity, long cycle life, high diffusion rate, cost effective, and non-toxic, are considered as suitable electrode material for lithium-ion batteries [19] .

1.3.4.1 Cathode

A desired cathode material for a lithium-ion battery is the one which has "a high discharge capacity, high energy capacity, long cycle life, high power density, low self-discharge, sufficiently high voltage and non-hazardous".

The first layered transition metal oxide cathode to be discovered was LiCoO2 by John B. Goodenough and continue to be used in most of the commercial Li-ion batteries [21]. With cobalt and lithium ions occupying alternate layers of octahedral sites and cubic closed packed oxygen atoms, the compound has a hexagonal symmetry. LiCoO2 (LCO) has a very high and desired theoretical volumetric capacity of 1363 mAh-cm^{-3}. Additionally, it also possesses a specific capacity (theoretical) of 274 mAh-g^{-1}. It also possesses other desirable characteristics such as superior cycling performance, more voltage discharge and reduced self-discharging. LCO has a sloping potential profile in lithium half cells and below the voltage of 4.2V vs. Li/Li^{+}, almost lithium ions are partly removed which results in high specific capacity [21, 23]. Higher capacities could be attained using LCO as a cathode material but it also steers structural instability due to de-intercalated LixCoO2. Being a limited resource, cobalt costs very high and this makes LCO cathodes expensive. LCO cathodes also possess lowest thermal stability compared to other transition metal oxide cathodes. At temperatures of over 200 °C, LCO cathodes suffer from thermal runaway due to exothermic

reactions between organic materials and released oxygen. This sets a limitation on the use of LCO as the cathode material [24].

Table l. l. Specific capacity, volumetric capacity and average potentials of Intercalation cathode materials [23]

Crystal Structure	Compound	Capacity per unit Volume (mAh-cm^{-3})	Specific capacity (mAh-g^{-1})	Average Voltage (V)
Layered	$LiTiS_2$	697	225/210	1.9
	$LiCoO_2$	1363	274/148	3.8
	$LiNiO_2$	1280	275/150	3.8
	$LiMnO_2$	1 148	285/140	3.3
	$LiNi_{0.33}Co_{0.33}Mn_{0.33}O_2$	1333	280/160	3.7
	$LiNi_{0.8}CoO_{0.15}A1_{.05}O_2$	1284	279/199	3.7
	Li_2MnO_3	1708	458/180	3.8
Spinel	$LiMnO_4$	596	148/120	4.1
	$LiCo_2O_4$	704		4.0
Olivine	$LiFePO_4$	589	170/165	3.4
	$LiMnPO_4$	567	171/168	3.8
	$LiCOPO_4$	510	167/125	4.2
Tavorite	$LiFeSO_4F$	487	151/120	3.7
	$LiVPO_4F$	484	156/129	4.2

1.3.4.2 Anode

Lithium metal, despite of highest capacity (3860 mAh-g^{-1}), is not preferred as an anode material because of dendrite formation leading to short circuit, thermal runaway, and other safety issues. Several efforts have been made to develop suitable anode materials with enhanced energy and power density without compromising with capacity, long cycle life, and ease of lithium-ion diffusion [24, 25]. Carbon based materials such as, carbon nanotubes (CNT), graphene, porous

carbon etc. have been probed for high capacity and improved performances. Non-carbon materials that have been investigated as anode for secondary batteries include silicon oxide (SiO), silicon (S), germanium (Ge), tin (Sn), and transition metal oxides. The major limitations for selection of anode materials are poor electron transport, capacity fading, high volume expansion and minimal value of coulomb efficiency, These limitations are overcome by nano-structuring the materials for effective use as anode [26-28]

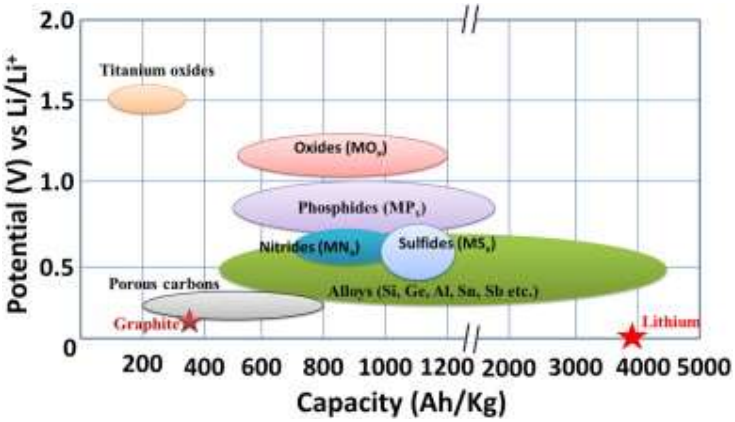

Fig 1.7 : Capacity vs Li/Li$^+$ potential[29]

Incorporating nanotech in lithium-ion battery development workflow results in substantial increase in capacity and elevated flux of lithium-ion across electrolyte and electrode interface. Reduction to nanoscale from bulk, leads to increased surface area which provides lithium storage at more functional sites and lithium diffusion rate increases due to decreased path length. The various innovative anode materials can be categorized into following types [29]:

(a) Intercalation and de-intercalation materials (carbon based materials, titanium dioxide, and LTO) (Details below).

(b) Alloy and de-alloy materials such as Silicon, Tin, Aluminium, and Tin Oxide,

(c) Conversion materials such as oxides of transition metals, MS_2 (Metal sulphides), MP (Metal Phosphides), and MN_3 (metal nitrides).

Intercalation/de-intercalation materials

Due to their good reversibility of lithium intercalation/de-intercalation, abundance in nature, stability in electrochemical and thermal environment, carbonaceous anode became commercially viable almost two decades ago, Since carbon displays electrical and chemical activity towards electrolytic solution at very low value of potentials, carbon coating on active materials prevent the active electrode material degradation as well as capacity fade upon charging and is charging and lessens the electrolyte's decomposition producing a thinner solid electrolyte interface film over the electrode [30]. Being chemically stable, Carbon coating provides protection against HF corrosion and surface oxidation in ease of nanostructured active materials. When graphite is carbon coated, it reduces the degradation of electrolyte and does not allow any electrolyte species to intercalate into the graphene layers. Similarly, carbon coating the LTO electrodes, helps reduce electrolyte decomposition. For silicon and germanium anodes, carbon coating led to improved battery performances [31, 32].

In carbon based materials, a single Li-ion intercalates with carbon atoms, six in number, resulting into a lithiated compound LiC_6. Carbon based materials can be categorized into two types: soft carbon (graphitic) and hard carbon. In graphitic carbons, unidirectional piling of the crystallites is observed where as in hard carbons, they have a disordered orientation. With large graphite grains, soft carbons can attain their theoretical capacity (372 mAh-g^{-1}). But due to the low value of the reversible capacity, they have their application limited to low power devices such as mobiles and laptops etc. [33, 34]. The major drawback of using graphitic carbon as an anode material is that propylene carbonate (electrolyte) tends to intercalate along with the Li-ions and causes exfoliation and capacity

fading. Also during lithium insertion, graphitic carbon experience strain in their crystal structure which results in decreasing the cycle life of the cell. Surface coating with amorphous carbon helps achieve superior coloumbic efficiency. The various commercially available graphites are Massive Artificial Graphite (MAG), Mesocarbon Microbead (MCMB), and carbon fiber-vapor grown (VGCF) etc. Development of nano-fibers, porous carbon, CNT, and graphene as a suitable carbon derived anode material is under research. These materials are expected to impart novel properties and increase the energy storage capacity of the secondary batteries [35, 38].

Hard carbons having disordered orientation tend not to undergo exfoliation upon lithiation. Compared to the soft carbon they possess much higher theoretical capacity (500 mAh-g^{-1}) in the potential range 1.5V vs. Li/Li^+. Due to random alignment of graphene sheets in hard carbon, nanovoids are present in between them which permits reduced and identical volume expansion in every direction. However, these voids lead to slow diffusion of Li-ions and thus inferior rate capacity. Low tap density and initial coulombic efficiency are considered to be the major drawbacks associated with hard carbon anodes. Coating of hard carbon with a fine film of metal film or soft carbon improves the coloumbic efficiency and the capacity to store lithium. Enhanced rate capability (approx. $4.11x10^{-5}$ $\frac{cm^2}{s}$) and cycle life were observed when nano-porous hard carbon materials were synthesized [37-39].Carbon nanotubes (CNT) produce superior results when used in association with other active anode materials, because of their extraordinary thermal and mechanical stability, adsorption, electronic conductivity, and transport properties. SWNT's can achieve theoretical capacity reaching up to 1163 mAh-g^{-1} for LiC_2 compound. This is because the lithium ion diffuses into stable surface sites of quasi graphitic layers, as well as within the tube. Certain nanostructured materials or oxides (M_xO_y: M = Cr, MO, Mn, Cu, Ni, and Fe) when coupled with carbon nanotubes, improve the serviceability of the battery

and its storage capacity of the lithium ions. Synthesis of such hybrid anode materials result in CNT's which reduces the changes in volume observed during the discharge cycle and charge cycle processes. Fan et al. stated that "CNT's with a coating of Fe_3O_4 displayed a capacity of 800 mAh-g^{-1} for 100 charge-discharge cycles and also improved rate capability" [40].

With superior properties like high mechanical strength, high values of charge mobility and surface area, along with good electrical conductivity it makes a very significant anode material to be used in Li-ion batteries. When several layers of graphene is taken into account, the amount of absorbed lithium is significantly huge and therefore, and as a consequence the capacity associated with the Li_2C_6 stoichiometry is 780 mAh-g^{-1} and 1116 mAh-g^{-1} with LiC_2. Li_2C_6 is formed when lithium ion interacts and get absorbed on both the faces of the graphene sheets. LiC_2 results when lithium is trapped in a covalent bond of a benzene ring. Pan et al. reported graphene sheets synthesized using low temperature pyrolysis, reduction process of hydrazine and electron beam irradiation. The graphene sheets when analysed electrochemically, established and displayed high gravimetric capacity ranging from 790 to 1050 mAh-g^{-1}.

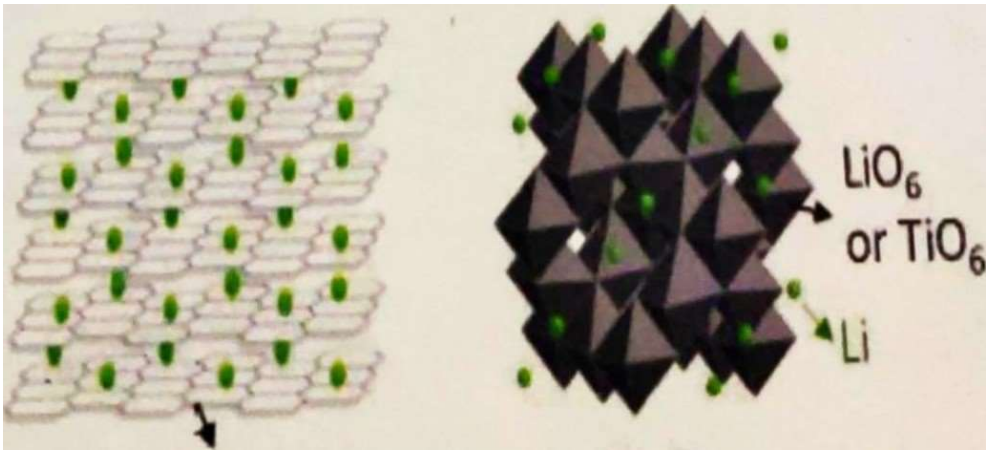

Graphite $Li_4Ti_5O_{12}$

Figure 1.8. Crystal structure of lithiated graphite and LTO[41]

Another important intercalation/de-intercalation anode material are titanium based oxides i.e. Lithium titanium oxide (LTO/ $Li_4Ti_5O_{12}$) and titania (TiO_2). These most important characteristics of these materials which make them suitable anode materials are inexpensive, non-toxic, nominal volume change upon charging and discharging and extended cycle life. Compared to their counterparts they have low theoretical capacity and electrical conductivity. However, with size reduced to nanoscale, these materials show improved capacity, longer cycle life, and efficient rate capability. The main reason of stability of these anodes is the 'zero strain' intercalation mechanism LTO. Lithiation/de-lithiation in LTO anodes causes very small volume change as a result they are considered to be 'zero strain' materials. The SEI formation in LTO anodes is also inhibited because of the high equilibrium potential voltage of approx. 1.55V vs. Li/Li^+ that permits the operation marginally above 1 V. LTO anodes are also considered to be tremendously safe. The cause for its high potential prevents Li dendrite formation. Consequently, they are considered suitable for high power, low energy and high cycle life lithium-ion batteries *[42, 43]*.

Table 1.2. Comparison of characteristics of different anode materials [43]

Material	D (cm^2 s^{-1})	De-lithiation potential (V)	Lithiation potential (V)	Volume change
Graphite	10^{-11}-10^{-17}	0.1, 0.14, 0.23	0.07, 0.10, 0.19	
LTO	10^{-12}-10^{-11}	1.58	1.55	0.2 %
Silicon	10^{-13}-10^{-11}	0.34, 0.57	0.05, 0.21	270 %
Germanium	10^{-12}-10^{-10}	0.5, 0.62	0.2, 0.3	240 %
Tin	10^{-16}-10^{-13}	0.58, 0.7, 0.78	0.4, 0.69	255 %
Li_2O	$5x10^{-12}$--$5x10^{-10}$	N/A	N/A	N/A

Chapter 2

Literature Review

Lithium iron phosphate ($LiFePO_4$) is arguably the most famous member of olivine-type lithium-metal phosphates i.e. $LiMPO_4$ (M = transition metal). Padhi et al. proposed the electrochemical extraction of lithium from $LiFePO_4$ in 1997 [44, 45, 46, 47]. Olivine structured $LiFePO_4$ (LFP) belongs to *Pnma* space group with orthorhombic lattice structure. Phosphor atoms in PO_4^{3-} unit occupies tetrahedral *4c* sites while iron cations in FeO_6 and lithium cations present in LiO_6 octahedral units occupies *4c* and *4a* sites, respectively [46, 48]. LFP unit cell contains four units of $LiFePO_4$ with 28 atoms in total [47]. The lattice parameters are given as *a*=10.33 Å, b=6.01 Å, c=4.69 Å with a volume of 291.2 $Å^3$ [49] . The oxygen atoms shared by the FeO_6 octahedron presents at the corner in the *bc* plane and PO_4 forms a zigzag structure while being present on edges. Phosphate unit (PO_4) shares the edges with two LiO_6 and one FeO_6 octahedron. LiO_6 grows as a linear chain along the *b* axis (i.e. [010] direction) in which Li ions present at octahedral sites as shown in Figure 2.1 [47, 47, 49]. The entire LFP framework is stabilised by the strong covalent bonding between phosphorus and oxygen in PO_4^{3-} tetrahedral structural unit. The presence of strong covalent bonds make it difficult to remove oxygen atoms from the structure which thus guarantees the excellent thermal stability

even up to 400 °C as compared to the layered cathode material such as $LiCoO_2$ which starts to decompose at 250 °C [44, 49]. In such a structure, edge shared LiO_6 forms a one-dimensional tunnel which contains mobile lithium ions [50]. The strongly bonded phosphorous, oxygen and transition metal linkage tunes the M^{3+}/M^{2+} redox potential to practical and stable voltage plateau [51]. However, the presence of such strong covalent bond is also responsible for poor electronic conductivity in pristine LFP [49]. It has been reported that in olivine structure, oxygen atoms show slightly distorted hexagonal close packed (hcp) arrangement from the actual structure [47,50, 52]. This deviation from ideal hcp arrangement has been correlated with Coulomb repulsion between cation-cation across the shared edges [53, 54].

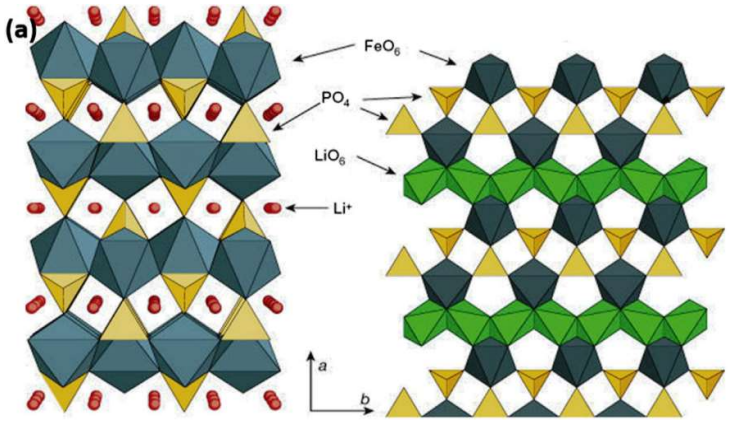

Figure 2.1: *Crystal structure of olivine $LiFePO_4$ [45]*

Rakesh Saroha et al [55] have performed experimental analysis of LFP and Ni doped LFP**.** The **v**arious ratio of Ni were mixed/doped in $LiFePO_4$ to make it as partial replacement of site in LFP as well as whole Fe to make it $LiNiPO_4$ as complete substitution of Ni and the properties were analysed. LFNPx. i.e.

$LiNi_xFe_{1-x}PO_4$ was synthesised by wet milling method. For electrochemical studies, Conductive carbon, polyvinylidene difluoride (PVDF) was mixed in 70.00:15.00:15.00 weight ratio in N-methyl-2pyrrolidinone (NM2P) and then coated on an aluminium foil current collector. Electrochemical Impedance spectroscopy has been performed in frequency range 0.01 Hz to 10^4 Hz at 5mV peak voltage amplitude. Out of these, the 3% ratio, i.e. LFNP3 was found to be the best case with an experimental yield confirmed to be of 92% of theoretical value. Average particle size was found to be around 50nm. The decrease in grain size results in enhanced electrochemical performance, because the diffusion length, diffusion coefficient and relaxation time are related as:

$$L = \sqrt{D\tau} \quad 2.1$$

Thus, a small decrease in L will result in decrease τ, hence, superior electrochemical performance. LFNP3 has low AC and DC resistance (~500 Ω) [55]. The nyquist plot contains a semicircle for high frequency region whereas the low frequency region is a straight line.

D.P. Abraham et al [56] modelled a 1D lithium battery with $LiNi_{0.8}Co_{0.15}Al_{0.05}O_2$ as cathode and performed electrochemical impedance spectroscopy in 10 mHz to 10kHz range of applied AC voltage, against a graphitic anode. 4 parameters , namely , positive particle radius, positive electrode double layer capacitance, Diffusion coefficient were varied and best fit data was obtained corresponding to experimental data obtained by Abraham et al[56] .

Thi Hang, La. et al [57] studied Nickel Doped lithium iron phosphate and studied its electro-chemical properties. Thus reporting significant performance improvements in the battery performance.

Rosaiah, P & Padarti[58] Studied Electric and dielectric properties of Nano crystalline $LiFePO_4$ over a frequency range of 1 Hz – 1 MHz at different temperatures and the electrochemical characteristics of $LiFePO_4$ in aqueous

region.. They found that the conductivity was proportional to temperature in accordance with Arrhenius relation with an estimated E_a = 0.44 eV ($7x10^{-20}$ J). Also, the authors analysed dielectric properties in light of complex dielectric permittivity. And thus, the behaviour of complex permittivity as a function of frequency and temperature was analysed. Authors found variation of permittivity by an order of magnitude over the frequency range.

M. Schönleber et al[59] derived the fundamental impedance of a LIB electrode [59] and additionally, the theoretical expected behaviour of charge-transfer and solid-state diffusion on the state of charge[54]. The derived impedance model has of an RC-element signifying charge-transfer, a Finite-Length Warburg element equivalent for diffusion in the electrolyte and a Finite-Space Warburg element for solid-state diffusion.

Y.-J. Lv et al[60] prepared $LiFePO_4$ cathode sample with a powder-to-ball weight ratio of 1:0.04 which was mostly composed of particles of size ~50nm. Electrochemical tests indicated that the sample thus synthesised had a discharge capacity of 125 mAh-g^{-1}. [60]

L. Dimesso et al [61] reported that the structural, electrochemical and morphological properties of nickel doped composites of Lithium of form $LiNi_yPO_4$ are strongly dependent upon the Nickel content. The X-ray diffractograms of showed formation of $LiNiPO_4$ phase with $Li_2Ni_3(P_2O_7)_2$ and $Li_4P_2O_7$. The specific capacity of the composites increased, reaching a peak value of 122 mAh-g^{-1}. [61]

J.P. Meyers et al [62] developed a model by taking into consideration, a porous electrode without the limitations imposed by solution-phase diffusion. The impedance response of a single particle with intercalation was derived by solving a set of governing equations. These equations describe solid-phase diffusion inside the particle, charge-transfer and double-layer charging at the surface, and

an open-circuit potential which is a function of intercalant concentration. The model also assumed that the intercalating particle has an insulating film surrounding it.

H. Schichlein et al [63] measured electrochemical impedance spectra at single cells for studying the polarisation at electrode-electrolyte interfaces. The single cells were based on a 0.15 μm thick, 8 mol % Yt doped zirconia substrate (8YSZ) with a size of 50 mm x 50 mm [63]. The electrical impedance of planar single SOFC elements was measured under realistic working conditions.

Chapter 3

Battery Modelling

3.1 Current Balance

The Lithium-Ion Battery Interface in COMSOL defines the current balance in the electrolyte, the current balances in the electrodes, the mass balance for the lithium salt, and the mass balance of lithium in lithium-ion batteries [44].

The electrolyte in battery should be a binary electrolyte, containing lithium cations (Li^+) and anions (An^-).

The physics interface in COMSOL solves for five dependent variables:

- ϕ_s , the electric potential,
- ϕ_l , the electrolyte potential,
- $\Delta \phi_{s,film}$, the potential losses due to a solid-electrolyte interface (SEI), the film forming on electrode particles
- c_s, the concentration of Li in the electrode particles, and
- c_l, the electrolyte salt concentration.

Assuming electro-neutrality, two variables, ϕ_l and c are defined in the electrolyte and pore electrolyte. Here c_l denotes both the Li^+ concentration and the An^- concentration. The electrolyte domain equations deal with the conservation of current and the salt mass balance:

$$\nabla . \left(-\sigma_l \nabla \phi_l + \frac{2\sigma_l RT}{F}\left(1 + \frac{\partial \ln}{\partial \ln c_l}\right)(1 - t_+)\nabla \ln c_l\right) = i_{tot} + Q_l \quad \text{- 3.1}$$

$$\frac{\epsilon_l(\partial c_l)}{\partial t} + \nabla . (-\epsilon_l D_l \nabla c_l) = R_l - \left(\frac{i_{tot}+Q_l}{F}\right) t_+ \quad \text{-3.2}$$

Where f is the activity coefficient for the salt, t_+ the transport number for Li^+ (also called transference number), σ_l denotes the electrolyte conductivity, i_{tot} the sum of all electrochemical current sources, and Q_l denotes an arbitrary electrolyte current source. In the mass balance for the salt, ε_l denotes the electrolyte volume fraction, D_l is the electrolyte salt diffusivity, and $R_{l\ is}$ the total Li^+ source in the electrolyte.

If σ_s is electrical conductivity, then, in the electrode, the current density, I_s, is defined as

$$i_s = -\sigma_s \nabla \phi_s \quad \text{-3.3}$$

The conservation of current in electrode is expressed as

$$\nabla i_s = -i_{tot} + Q_s \quad \text{-3.4}$$

Where Q_s is the arbitrary current source term.

The state-of-charge variable for the solid particles in lithium electrodes is denoted ‘soc’. This is defined as

$$soc = \frac{c_s}{c_{s,max}} \quad \text{-3.5}$$

For lithium insertion electrode reactions, equilibrium potentials E_0 are usually dependent on soc. The electrode reaction occurs on the particle surface and lithium diffuses to and from the surface in the particles. A continuity equation can depict the mass balance of Li as:

$$\frac{\partial c_s}{\partial t} = \nabla . (-D_s c_s) \quad \text{-3.6}$$

Where D_s is the diffusion coefficient for lithium in cm^2-s^{-1}.

3.2 Film resistance

An additional potential losses in the electrodes can be attributed to a resistive film that might form on the solid particles this is also called solid-electrolyte interface,or, SEI). For including this film resistance in model, a variable for the potential variation arcoss the film, $\Delta\phi_s$, film, is introduced in the physics interface. Then,according to ohm's law,

$$\Delta\phi_{s,film} = i_{tot} R_{film} \quad \text{-3.7}$$

where R_{film} ($\Omega \cdot m^2$) is a generalized film resistance. This potential contributes to the activation over-potentials, η_m, for all electrode reactions in the electrode, which yields

$$\eta_m = \phi_s - \Delta\phi_{s,film} - \phi_l - E_{eq,m} \text{ [73]} \quad \text{-3.8}$$

If the thickness and conductivity of the film are known, the resistance can be written as:

$$R_{film} = \frac{s_0 + \Delta s}{\sigma_{film}} \quad \text{[74]} \quad \text{-3.9}$$

where s_0 is the reference/initial film thickness, Δs the electrode thickness change, and σ_{film} the conductivity (S/m) of the film.

3.3 Initial Charge Distribution in The Battery Cell

The number of parameters in battery models are many but especially setting the charge distribution in the cell, i.e. the intercalating species concentration in each electrode material, is not always straight forward since it often requires more detailed information than just cell voltage and capacity. It is, however, possible to compute the initial charge distribution taking into account that initially, when no current is applied on a battery cell and no sources of polarization apply, it is only the difference between the positive and negative electrode material

equilibrium potentials that dictates the cell voltage. Two constraints can be set up with the battery cell capacity and voltage as inputs for this computation:

From law of conservation of charge, the battery cell capacity, $Q_{cell,0}$ (C), is equal to the sum of the charge of cycle-able species, $Q_{cycl,}$, in positive and negative electrodes.

$$Q_{cell,0} = Q_{cycl,pos} + Q_{cycl,neg} \quad [75] \qquad -3.10$$

The capable species charge in an electrode is defined as :

$$Q_{cycl,electrode} = c_{s,avg,electrode} \int_{\Omega_s} F \epsilon_s d\Omega \qquad -3.11$$

Where, ε_s denotes the electrode volume fraction and $c_{s,avg,cycl,electrode}$ is the local average cycle-able species concentration defined as:

$$c_{s,avg,cycl,electrode} = c_{s,avg,electrode} - soc_{min} c_{s,max} \qquad -3.12$$

The electrode potential is constant in each electrode and the difference between the electrode potentials is equal to cell voltage.

$$E_{cell,0} = \frac{\int_{\Omega} \phi d\Omega_s}{\int_{\Omega} d\,\Omega} - \frac{\int_{\Omega_s} \phi_s d\Omega}{\int_{\Omega_{avg}} d\Omega} \quad [75] \qquad -3.13$$

Initially, when no polarization is present in the cell, the expression is equal to difference in the open-circuit potential of the electrode materials, E_{eq}:

$$E_{cell,0} = E_{eq,pos}(soc_{pos,0}) - E_{eq,neg}(soc_{neg,0}) \quad [75] \qquad -3.14$$

The cell voltage is restricted to the open-circuit potential of the electrode materials and the cell voltage should be set within the following range:

$$E_{eq,pos}(soc_{max}) - E_{eq,neg}(soc_{\min}) \leq E_{cell,0} \leq E_{eq,pos}(soc_{min}) - E_{eq,neg}(soc_{max}) \qquad -3.15$$

The expression for the electrode volume fraction in each electrode is given by:

$$\epsilon_s = \frac{Q_{host,electrode,0}}{\int_{\Omega_{electrode}} \Delta soc.C_{s,max} F d\Omega} \quad [75] \qquad \text{-3.16}$$

Where $Q_{host,electrode,0}$ (C) is the amount of active host material, Δsoc is the allowed state-of-charge window of the electrode material.

3.4 Electrode Kinetics Equations

For an electrode reaction, the activation over-potential, denoted η, is defined as follows:

$$\eta = \phi_s - \phi_l - E_{eq} \ [73] \qquad \text{-3.17}$$

where E_{eq} denotes the equilibrium potential.

3.4.1 Butler-Volmer[64]

The most general expression is of Butler-Volmer type [64]:

$$i_{loc} = i_0 \left(\exp\left(\frac{\alpha_a F \eta}{RT}\right) - \exp\left(\frac{-\alpha_c F \eta}{RT}\right) \right) \qquad \text{-3.18}$$

where α_c and α_a denote the cathodic and anodic charge transfer coefficient respectively.

For small overpotentials ($\eta << RT/F$) and the expression is a linearized Butler Volmer expression and is usually referred to as the low-field approximation

$$i_{loc} = i_0 \left(\frac{(\alpha_c + \alpha_a)F}{RT}\right) \eta \qquad \text{-3.19}$$

3.4.2 Limiting Current Density

The steady-state rate of electrode reactions never exceeds the rate at which reactants and products can be transported to and from the electrode surface. When

explicitly including mass transport in a model, this dependence is typically described by a concentration dependent kinetics expression as described below :

$$i_{loc} = i_0(C_r \exp\left(\frac{\alpha_a F\eta}{RT}\right)) \quad \text{-3.20}$$

3.5 Electrochemical Impedance Spectroscopy

Electrochemical impedance spectroscopy (EIS) is a valuable method to investigate electrochemical systems such as batteries. For a battery, where potential perturbations of varying frequency are applied on an electrode, the impedance response can give critical insights in battery processes as:

- Capacitance, electrochemical reactions, and local resistances which are short time-scale processes affect the impedance at high frequencies. [41]
- Whereas, at low frequencies, diffusion in the electrolyte and active material particles (i.e. , large time-scale processes) contribute to the impedance.[42]

3.6 Non-Linear Battery Impedance Model

Due to its accuracy and non-damaging effects, Electrochemical impedance spectroscopy (EIS) is a very feasible and also the most preferred method for obtaining the impedance characterization of Li-ion batteries, For EIS, a sinosuidally varying potential at different frequencies, but fixed peak-to-peak voltage is applied across the battery terminals, the output response is a function of frequency and can be studied using any frequency domain analysis tools[43].

For low frequencies, the resistances dominate over other transient elements such as capacitances, thus, impedance spectroscopy looks like a straight line with a

constant slope. In the mid-frequency region, the RC equivalent for battery comes into play and the impedance spectroscopy mimics the phasor plot of a RC circuit, which is a depressed semicircle in first quadrant. This is caused by the charge transfer reaction at the electrode surfaces. For the high-frequency region, the impedance spectroscopy forms a small curve and intersects with the abscissa axis. The high-frequency region reflects the battery's inductance and ohmic resistance. The electrical equivalent model thus consists of three parts to represent the physical and electrochemical reaction processes inside the battery. The conductive resistance. And a capacitance connected in parallel with a resistance for each electrode to simulate the double layer capacitance and Interfacial resistance. [65,66]

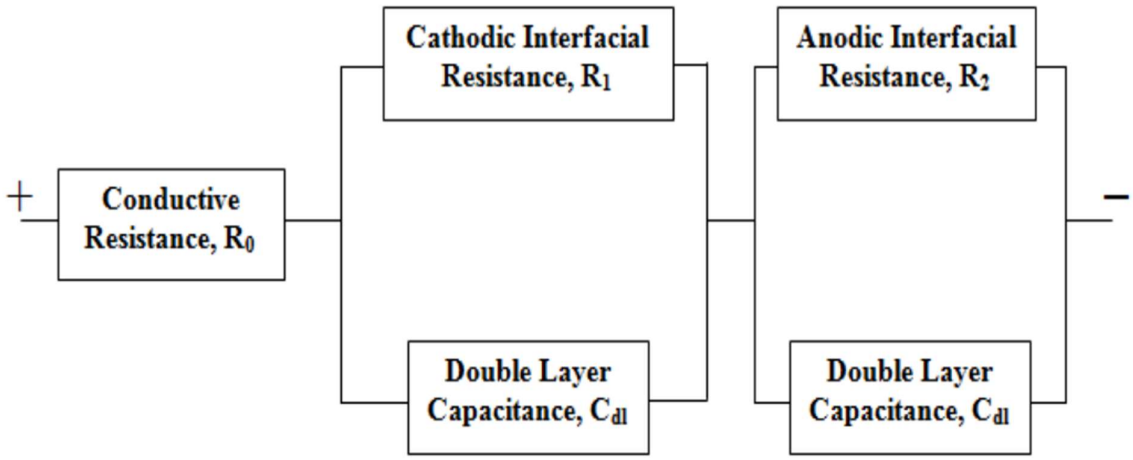

Figure 3.1: Equivalent circuit model of battery [67,68]

3.7 NYQUIST PLOT

Nyquist plots are representation of frequency dependent entities such as impedance, voltage gains, system transfer functions in complex plane in polar co-ordinates [67]. Nyquist plots are essential in complex frequency analysis. A lot of information can be readily derived from a Nyquist plots such as loss tangent, DC and AC responses. The impedance in polar form can be represented as, where Z'

is Real(Z) (resistance) and Z'' is imaginary part of impedance (capacitive reactance).

$$Z = Z_0 e^{i\theta} \quad \text{-3.21}$$

$$Z_0 = |Z' + iZ''| \quad \text{-3.22}$$

$$\theta = \tan^{-1}\left(\frac{Z''}{Z'}\right) \quad \text{-3.23}$$

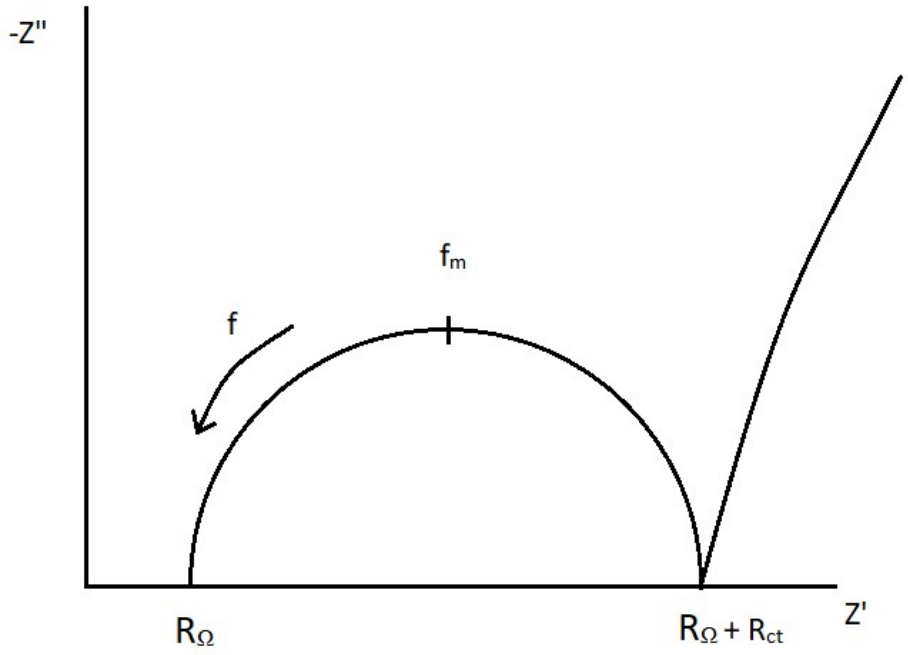

Fig 3.2: A sample Nyquist plot of lithium ion battery

In this simulation and modeling study, the material data was taken from given default materials in the program libraries, the experimental material data of Rakesh Saroha et al [55] for LFP and Ni doped LFP as cathode materials and Abraham et al [56], for graphitic carbon-based anode. Moreover, for electrochemical impedance spectroscopy analysis for pristine LFP and Ni doped LFP data simulation, experimental data of Rakesh Saroha et al [55] has been used from raw dataset.

Chapter 4

Theoretical modelling and simulation of LFP & Ni doped LFP

4.1 Introduction

In this study, we have developed a simulated model by altering the parameters and materials in the frequency domain perturbation study of Lithium- ion Battery from the batteries module available in COMSOL Multi-physics. The cell geometry is a one-dimensional model set up, which is close enough to simulate a coin cell, due to the inherent symmetry of the cylindrical structure of cell. The present investigation aims to reproduce the results of Rakesh Saroha et al [55], using simulation methodology, which would be able to help and predict other properties of the cell assembly. The processes of charge and mass transport in solid and solution phase has been included in the constituted model. These processes include the electronic conduction, charge transport of ions in the electrodes & the electrolyte. The kinetics of porous electrode are intended for potential achieved at the time of equilibrium for material within the spherical particles. The model developed for this study has porous electrodes of LFP and Ni doped LFP in 1:1 EC:DMC electrolyte against another graphitic carbon electrode.

The graphitic carbon electrode material is the unaltered version of the default material available in COMSOL multi-physics. The properties of EC: DMC 1:1 were taken from product data sheets available on vendor website product listings.

4.2 Model Definition and Parameters

Fig 4.1 shows the model setup with all components and materials.

The geometry node consists of the physical definition of various parts of the battery. The materials node consists of the materials used in the model, and the Li-Ion Battery node consists of the various parameters in the battery such as the applied potentials and the intercalation properties of materials.

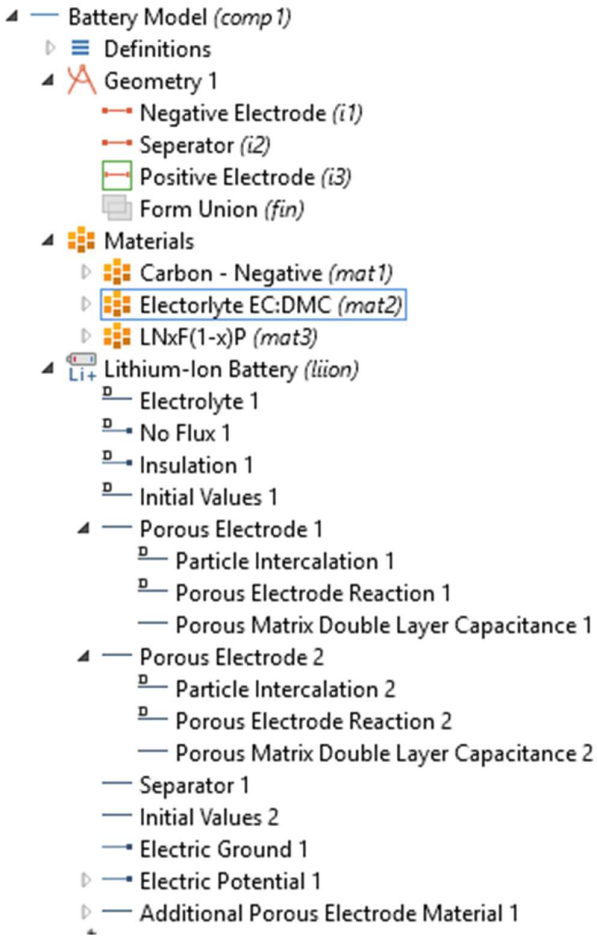

Fig 4.1 Model Setup –COMSOL Multiphysics

The positive electrode is a porous LFNPx (x denotes % of Ni doped in LPF) custom material and the negative electrode consists of LiC_6 where carbon is in graphitic form. During discharge, the porous electrode acts as the cathode and the current collector is the contact of the metallic tab, modelled here as exchange current density probe. The material and current balances in the lithium-ion battery are defined and solved using the model. A fourth independent variable for the particle radius is used to solve the insertion of lithium inside the particles in the positive electrode. The parameters used in the making of the model are listed below. The input values in the model were taken from the global parameter list as well as the material list of the model . Some parameters were also calculated using the experimental data, namely, electrode area, dielectric constant, conductivity, diffusion coefficients. The physical parameter of the coin cell such as the dimension of the electrodes, separator, and volume fraction were provided as an input in the model along with the electrode current. Some of these are:

1. Volumetric capacitance of electronic conductor in positive electrode
2. Film resistance positive electrode and negative electrode
3. Current collector area
4. Active material particle radius positive electrode
5. Exchange current density positive electrode

Probes to collect data from the model for above parameters were defined as shown in figure 4.2.

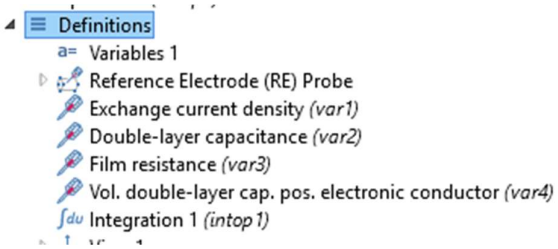

Fig 4.2 Probe Setup

4.3 Parameter Variation

Four parameters, which might change due to construction, testing and fabrication processes were varied in a parameter sweep study, which was subsequently fed into a frequency domain perturbation study.

These four parameters are:

1. Particle radius positive electrode (50-100 nm)*
2. Double layer capacitance on positive electrode (0.293 - 1 F/m^2)*^
3. Exchange current density (155-200 A/m^2)
4. Positive electrode film resistance. ($2.8x10^{-3}$ – $2.8x10^{-6}$ Ω – m^2)

- For a total of 8 cases.
* indicates the values calculated from Rakesh Saroha et al [55].
^ Value of Dielectric constant from Rosaiah et al [58]

The study was then fed into an optimisation study that compares the data obtained from different parameter sweeps and tries to fit it with experimental data from Rakesh Saroha et al [55].

Table 4.1 Parameter table for COMSOL Output

Parameters

Name	Expression	Value	Description
rp_neg	5e-7[m]	5E-7 m	Active material particle radius negative electrode
rp_pos	2.4911e-7[m]	2.4911E-7 m	Active material particle radius positive electrode
A_cell	32e-4[m^2]	0.0032 m^2	Current collector area
Rfilm_pos	2.848e-3[m^2/S]	0.002848 Ω·m^2	Film resistance positive electrode
L_neg	115e-6[m]	1.15E-4 m	Thickness negative electrode
L_pos	35e-6[m]	3.5E-5 m	Thickness positive electrode
L_sep	50e-6[m]	5E-5 m	Thickness separator

Table 4.2 Parameter Variation Table

Parameter name	Parameter value list
i0_pos (Exchange current density positive electr	180 200 180 180 180 180
cdl_pos (Double layer capacitance positive elect	0.2393 0.2393 0.5 0.2393 23.93 0.2393
Rfilm_pos (Film resistance positive electrode)	2.8e-3 2.8e-3 2.848e-3 1e-5 2.8e-3 2.8e-6
cdlvol_cs_pos (Volumetric capacitance of electr	2.557e5 2.557e5 2.557e5 2.557e5 1e4 2.557e5
rp_pos (Active material particle radius positive e	2.4911e-8 2.4911e-8 2.4911e-8 2.4911e-8 4e-8 4e-8

4.3.1 Current interface and Double layer capacitance setups

The secondary and tertiary current distribution in porous electrodes as set up as shown in figure

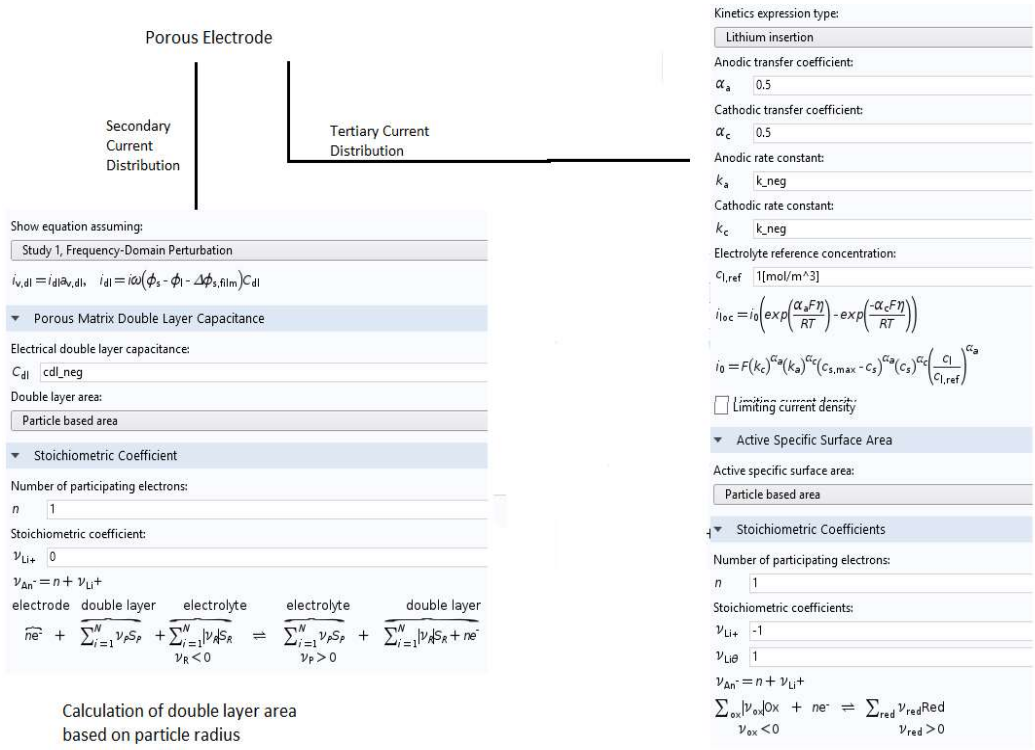

Fig 4.3: Double layer capacitance, Secondary and tertiary current setup

4.4 Results and Discussion

4.4.1 Parametric study results

Different Parameters of cell were varied as follows and the results were optimised for different concentrations for Ni in $LiNi_xFe_{1-x}PO4$

Table 4.3: Parameter Variation ranges and step sizes

Parameter	Unit	Max	Min	Step size
Positive Double Layer Capacitance	$\frac{F}{cm2}$	0.9	0.2	0.07
Film Resistance	Ω	2.5e-3	1e-6	100e-6
Particle Radius	Nm	150	50	10
Volumetric Capacitance	$\frac{F}{cm^2}$	2.57e5	2.57e4	1e4
Electrode state of charge	-	0.7	0.92	0.02
Diffusion Coefficient	$\frac{m^2}{s}$	7.16e-10	3.2e-13	7.15e-10

The result of parameter variation is summarised in table 4.4:

Table 4.4: Parameter Variation Results

Parameter	**LFP**	**LFNP3**	**LFNP5**	**LFNP7**
Double Layer Capacitance ($F\text{-}m^{-2}$)	0.5	0.83	0.3	0.05
Film Resistance (Ω)	$4.5x10^{-5}$	$2.8x10^{-5}$	$1.7x10^{-5}$	$0.5x10^{-5}$
Particle Radius (nm)	100	65	75	82
Volumetric Capacitance ($F\text{-}m^{-2}x10^5$)	2.577	2.34	2.20	1.78
State of Charge	0.89	0.92	0.87	0.82
Diffusion Co-efficient (m^2s^{-1})	7.34e-10	2.2e-13	1.16e-12	8.16e-10

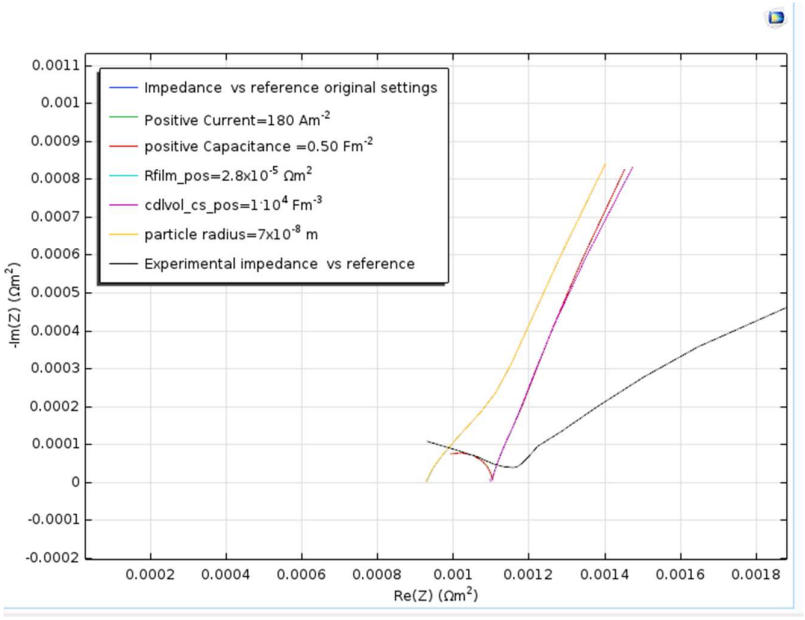

Fig 4.4 Effect of Different parameters variation result on Nyquist plot

The experimental data indicated presence of DC resistance as shown by the tilted low frequency plot in *fig. 4.4*. As, if there were zero dc resistance, it must be a straight, vertical line.

The High frequency plot shows the general form of phasor of a Resistor-Capacitor circuit. Which is indicative of the capacitance produced by electrochemical reactions and the charge transfer resistance. This is reproduced in the model and the data is brought to close fit via parameter variation.

The effect of variation of parameters on electrochemical impedance is as follows:

1. Increasing particle radius tends to depart from the mid frequency dip i.e. the Charge transfer resistance in imaginary component of impedance. This is evident in the graphs for LFP, LFNP3, LFNP5, and LFNP7.

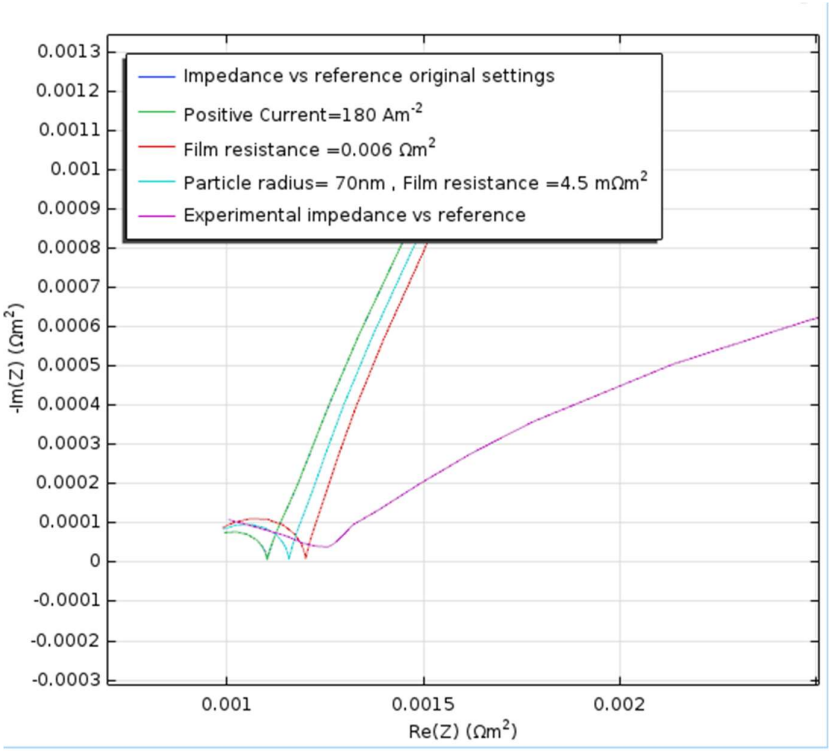

Fig 4.5 Effect of particle radius variation on impedance plot

This can be attributed to decrease in conductivity due to increase in particle size.

2. The positive film resistance alters the abscissa of the mid frequency dip, as well as the 'tilt' angle of the low frequency plot. The double layer capacitance and electrode capacitance play vital roles in showing the characteristic semi-circle phasor diagram in high frequency region.

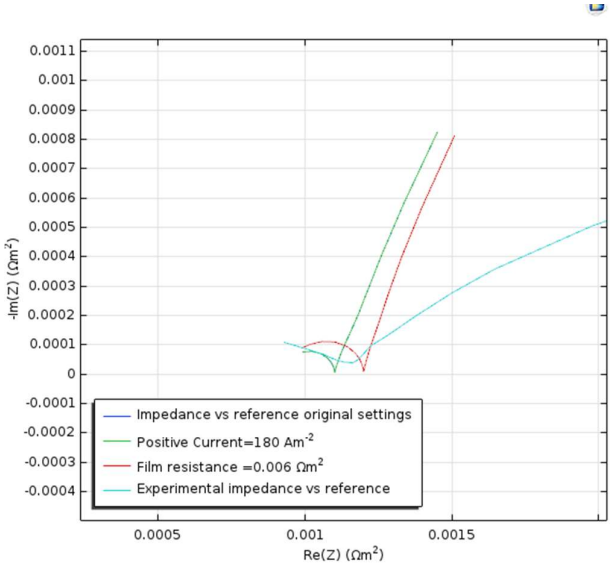

Fig 4.6 Effect of Varying film resistance on impedance plot

3. Change in current density has minimal effect on Nyquist plot, which is to be expected for the plot, i.e. impedance is independent of the current applied

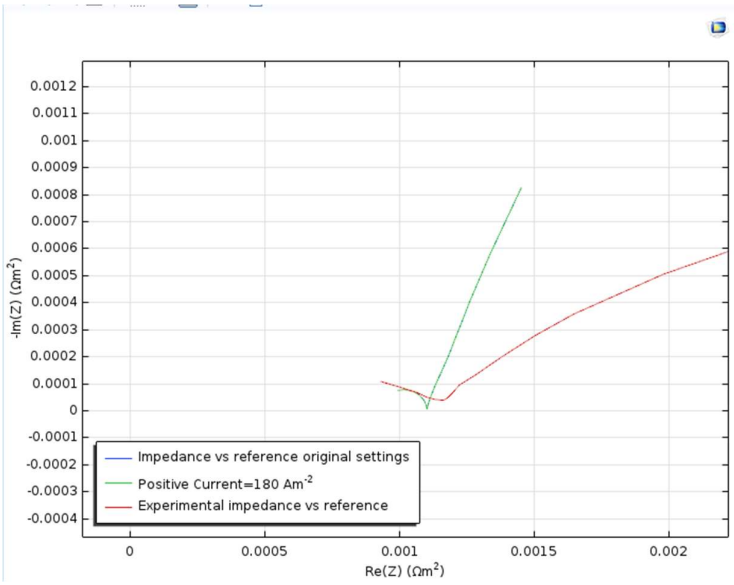

Fig 4.7 Variation of current having no effect on impedance plot

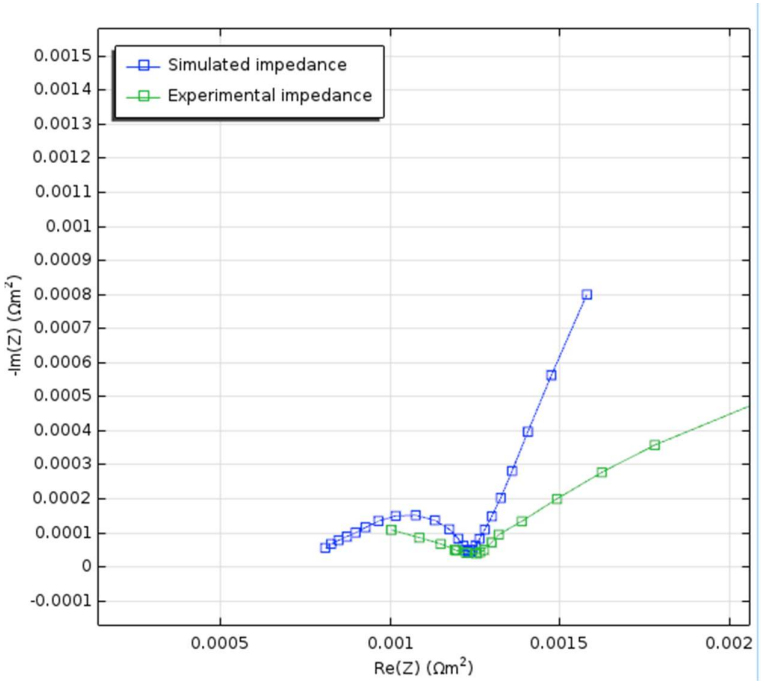

Fig 4.8 Optimisation for mid frequency range

The model varied the dependent parameters to fit for different ratios of Ni in LFP. The lowest value of charge transfer resistance was obtained for LFNP3, in accordance with experimental results by Rakesh et al[55]

4.4.2 Effect of change of doping percentage

The properties of LFP get significantly improved for low level doping of Ni, the best performance, i.e. electrochemical impedance occurring at 3% doping, i.e. LFNP3. On increasing the doping to 5% i.e. in LFNP5, the performance degrades with a significant increase (~98% , 48Ω to 92Ω Charge transfer resistance).

On further increase of doping, to 7% the charge transfer resistance increases beyond that of pristine LFP.

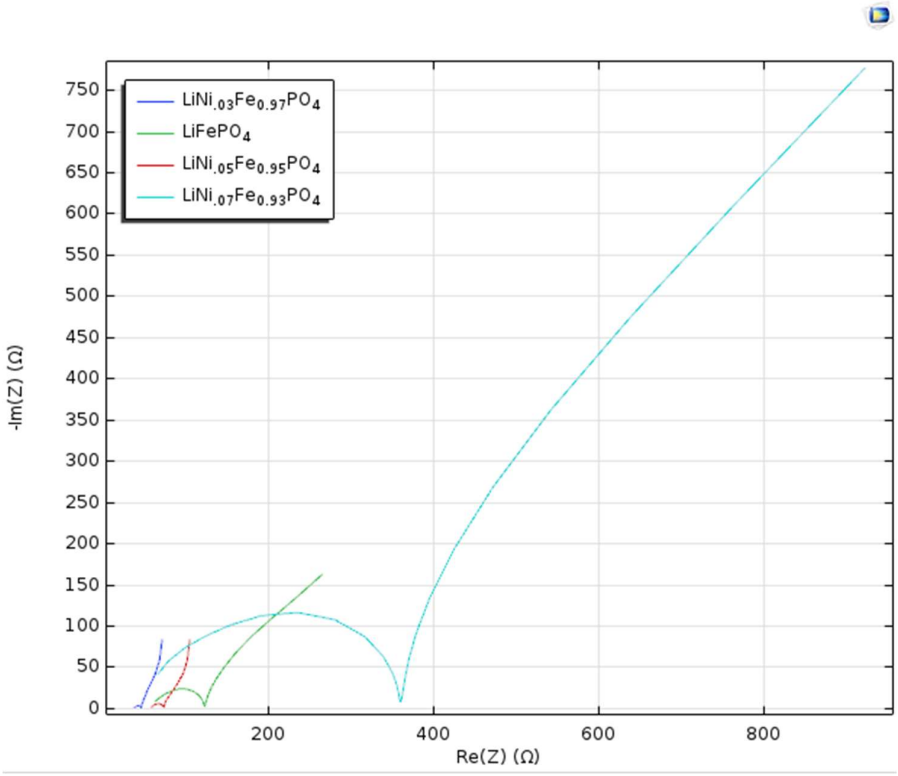

Fig: 4.9 LFP, LFNP3, LFNP5 and LFNP7 Impedance Spectra

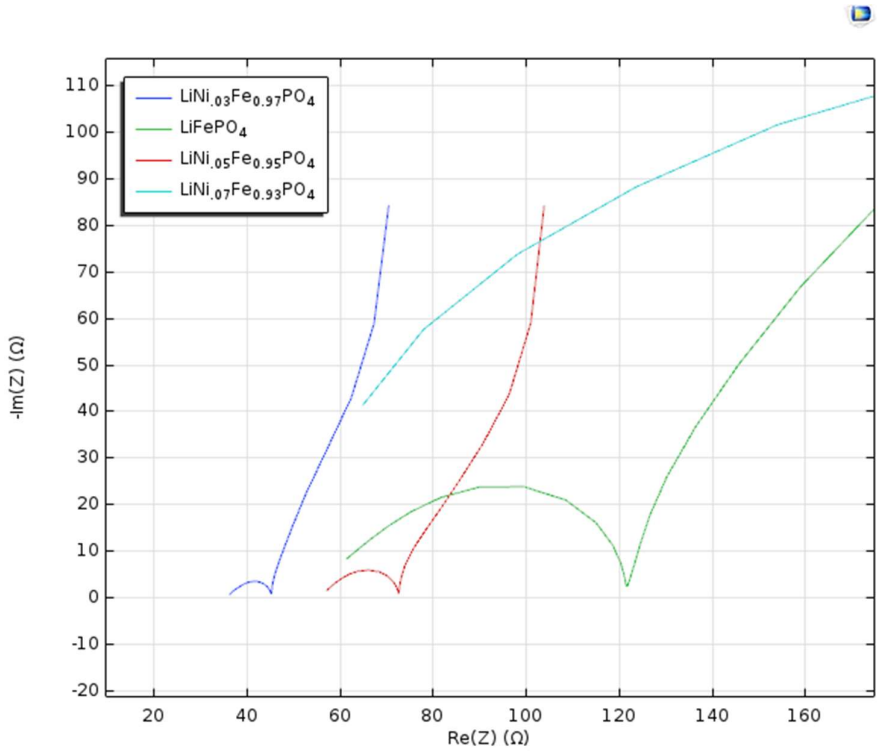

Fig 4.10 Zoomed in view for LFNP3 and LFNP5.

The Optimised parameters for LFNP3 are as obtained:

- Positive particle radius - 65 nm,
- Double layer capacitance - 0.83 F/m2 ,
- Volumetric Capacitance – 2.35×10^5 F/m2
- Film resistance $-2.8 \times 10^{-5} \Omega - m^2$
- Diffusion coefficient - 2.2e-13

As Compared to pristine $LiFePO_4$, LFNP3 has lower charge transfer resistance by almost half as shown by the graph, which is in confirmation with Rakesh et al [55]. LFNP3 has higher electrical conductivity (10^{-4} $\frac{S}{cm}$ to $10^{-9}\frac{S}{cm}$), smaller particle size and lower volumetric capacitances as shown by the impedance plot.

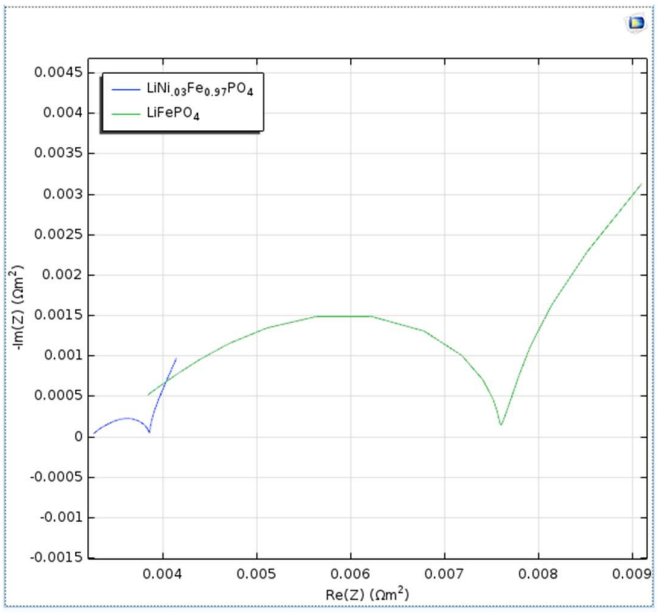

Fig 4.11 Performance of LFNP3 vs. LFP

Equivalent circuits for the half cell predicted by model:
The circuit of a cell consists of 2 capacitances, the double layer capacitance and volumetric capacitance in parallel, which are in series with a film resistance. This R-C circuit is in series with another resistance signifying the charge transfer resistance, which along with the film resistance signifies the conduction resistance.

LFP has a charge transfer resistance of 121 Ω, a double layer capacitance of 0.5 F-m^{-2} and a film resistance of 0.04 mΩ.

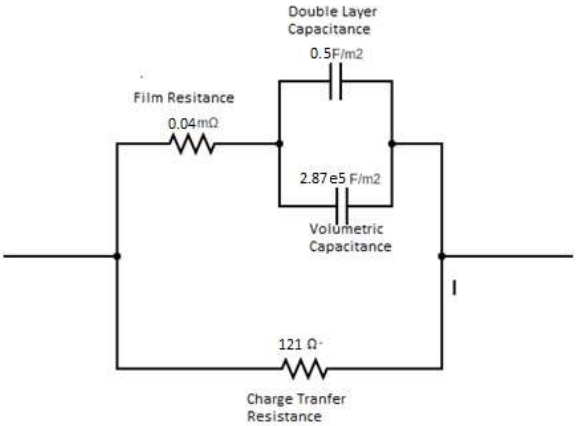

Fig 4.12 Equivalent circuit for LFP

In LFNP3, the resistance drops to 41 Ω, signifying the superior electrochemical performance.

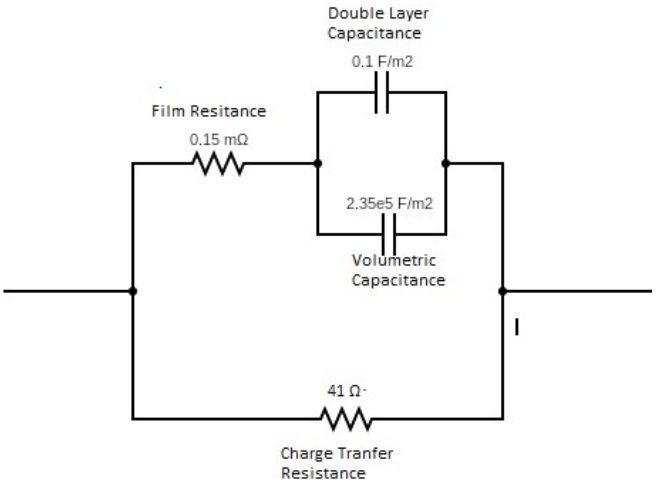

Fig 4.13 Equivalent circuit for LFNP3

On increasing the doping to 5%, i.e. LFNP5, the resistance increases, confirming an increase in particle radius and thus, decreased conductivity.

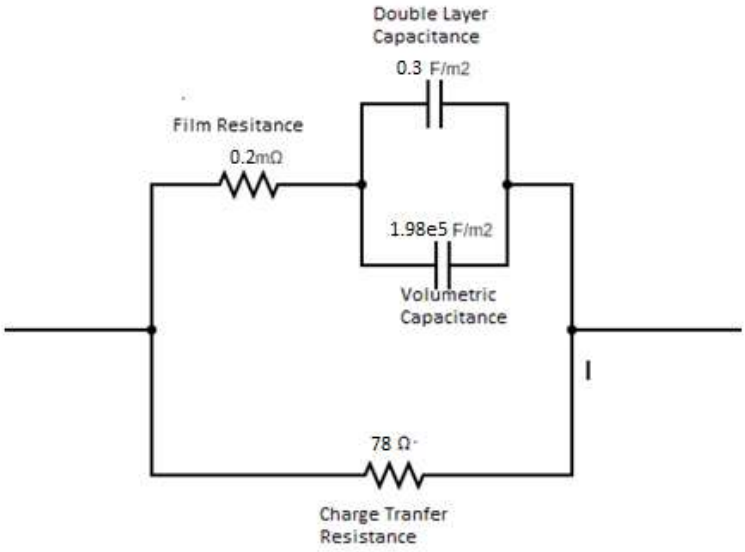

Fig 4.14 Equivalent circuit for LFNP5

In 7 % Ni doping, i.e. in LFNP7, the performance becomes worse than pristine LFP, with a large charge transfer resistance of 358Ω, showing an almost double increase from pristine LFP.

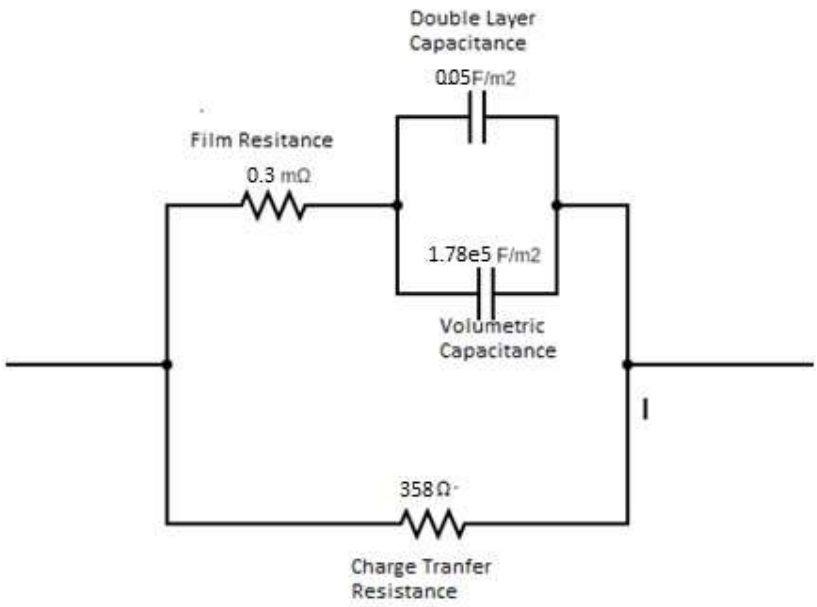

Fig 4.15 Equivalent circuit for LFNP7

Chapter 6

Summary and Conclusion

The theoretical model with optimised parameters is able to confirm the data from experimental data which, by correlation is a verification that the model, and by concomitance, the material profile is close to the actual model and parameters, and thus, may be used to predict the behaviour of cell with LFNP3 LFNP5 and LFNP7. The model agrees with the experimental data that LFNP3 is the most suitable drop in replacement for the pristine LFP, as evidenced by the optimised impedance model. On increasing the doping percentage, the parameters follow a similar trend, i.e. when compared to LFNP3 for other doping percentage the parameters which decrease (e.g. film resistance), keep on decreasing and parameters which increase (e.g. particle radius) keep on increasing and show increasingly poor performance.

Further, this model can be extended to also include the joule heating effect of current while charging and discharging and the subsequent change in battery parameters. The model parameter sweep can be adjusted to simulate additional fractions of doping after the optimised values are found out. Further, this can be extended to predict the electro-thermal performance of battery pack made from any of these materials.

References

1. Energy Transitions: History, Requirements, Prospects –Vaclav Smil ISBN-13: 978-0313381775
2. Nair, N. K. C., & Garimella, N. (2010). Battery energy storage systems: Assessment for small-scale renewable energy integration. Energy and Buildings, 42(1 1), 21242130.
3. Pistoia, G. (2005). Batteries for portable devices. Elsevier.
4. Bellis, M. (2008). Biography of Alessandro Volta—Stored Electricity and the First Battery. Google Scholar.
5. Oakes, E. H. (2014). A to Z of STS scientists. Infobase Publishing.
6. Functional materials analysis using in situ and it in operando X-ray and neutron scattering, Peterson, V. K. & Papadakis, C. M. (2015). IUCrJ 2, 292-304.
7. Linden, D., & Reddy, T. B. (2002). Handbook of Batteries. 3rd. McGraw-Hill.
8. Olivetti, E., Gregory, J., & Kirchain, R. (2011). Life cycle impacts of alkaline batteries with a focus on end-of-life. Study conducted for the National Electric Manufacturers Association.
9. Hooper, A., & Sequeira, C. A. (Eds.). (1985). Solid state batteries. Martinus Nijhofl
10. Linden, D. (2005). Batteries and Fuel Cells. Electronics Engineers' Handbook. „Edited by: DG Fink and AA McKenzie. McGraw-Hill Book co.. NY, 7-66.

11. Nelson, R. F., & Kepros, M. A. (1999). AC ripple effects on VRLA batteries in float applications. In Battery Conference on Applications and Advances, 1999. The Fourteenth Annual (pp. 281-289). IEEE.
12. Buthelezi, T., Dingrando, L., Hainen, N., Wistrom, C., & Zike, D. (2008). Chemistry': Matter and change. Glencoe/McGraw-Hill.
13. Mauger, A., & Julien, C. M. (2017). Critical review on lithium-ion batteries: are they safe? Sustainable?. Ionics, 23(8), 1933-1947.
14. Whittingham, M. S. (1976). Electrical energy storage and intercalation chemistry. Science, /92(4244), 1126-1 127.
15. Besenhard, J. 0., & Eichinger, G. (1976). High energy density lithium cells: Part l. Electrolytes and anodes. Journal of Electroanalytical Chemistry and Interfacial Electrochemistry, 68(1), 1-18.
16. Godshall, N. A. (1986). Lithium transport in ternary lithium-copper-oxygen cathode materials. Solid State Ionics, 18, 788-793.
17.. Yazami, R., & Touzain, P. (1983). A reversible graphite-lithium negative electrode for electrochemical generators. Journal ofPom,r Sources, 9(3), 365-371.
18. https://scipol.org/sites/default/files/diagram%20of%20lithium%20ion%20battery.png
19. Atoatucci, O. G., Tarascon. J. M., & Klein. L. C. (1996). C002 , The End Member of the li x coo2 solid solution. Journal of the Electrochemical society, 143(3)), 1114-1123.
20. Wakita S. Okac. 1. (2008). US Patent Application No. ///745,94/.
21. Murphy D. W. & Trumbore. F. A. (1976). The Chemistry of TiS3 and NbSe3 cathodes. Journal of Electrochemical Society, /23(7), 960-964.

22. Mizushima,K., Jones P.C., Wiseman, P,J,m & Goodenough, J. B. (1980), LixCoO2 (0<x<-1): A new Cathode material for batteries of high energy densitu. Materials Research Bulletin, 15(6),783-789

23. Zaghib, K., Julien, C. M., & Prakash, J. (Eds.). (2003). New Trends in Intercalation compounds for Energy Storage and Conversion: of the Intemational Symposium. The Electrochemical Society.

24. Du Pasquier, A., Plitz, I., Menocal, S., & Amatucci, G. (2003). A comparative study of Li-ion battery, supercapacitor and nonaqueous asymmetric hybrid devices for automotive applications. Journal ofPower Sources, 115(1), 171-178.

25. Williard, N., He, W., Hendricks, C., & Pecht, M. (2013). Lessons leamed from the 787 dreamliner issue on lithium-ion battery reliability. Energies, 6(9), 46824695.

26. Jiang, J., Li, Y., Liu, J., Huang, X., Yuan, C., & Lou, X. W. D. (2012). Recent advances in metal oxide-based electrode architecture design for electrochemical energy storage. Advanced materials, 24(38), 5166-5180.

27. Wang, Z., Zhou, L., & Lou, X. W. (2012). Metal oxide hollow nanostructures for lithium-ion batteries. Advanced materials, 24(14), 1903-1911.

28. Prosini, P. P., Carewska, M., Loreti, S., Minarini, C., & Passerini, S. (2000). Lithium iron oxide as alternative anode for li-ion batteries. International Journal of Inorganic Materials, 2(4), 365-370.

29. Bruce, P. G., Scrosati, B., & Tarascon, J. M. (2008). Nanomaterials for rechargeable lithium batteries. Angewandte Chemie International Edition, 47(16), 2930-2946.

30. Capiglia, C., Saito, Y., Kataoka, H., Kodama, T., Quartarone, E., & Mustarelli. P. (2000). Structure and transport properties of polymer gel electrolytes based on PVdF-HFP and LiN (C2F5S02) 2. solid state Ionics, 13/(3-4), 291-299.
31. Li, H., & Zhou, H. (2012). Enhancing the performances of Li-ion batt«ies by carbon-coating: present and future. Chemical Communications, 48(9), 1201-1217.
32. Aurbach, D. (2000). Review of selected electrode—solution interactions which determine the performance of Li and Li ion batteries. Journal of Power Sources, 89(2), 206-218.
33. Park, T. H., Yeo, J. S., seo, M. H., Miyawaki, J., Mochida, L, & Yoon, S. H. (2013). Enhancing the rate performance of graphite anodes through addition of natural Graphite/carbon nanofibcrs in lithium-ion batteries. Electrochimica Acta, 236240.
34. Haik, 0., Ganin, S, Gershinsky. G., Zinigrad, E.. Markovsky, B.. Aurbach, D., & Halalay. l. (201 1). On the thermal behavior of lithium intercalated graphites. Journal of The Electrochemical Society, 158(8), A913-A923.
35. Wang, H., Yoshio, M., Abe, T., & Ogumi, Z. (2002). Characterization of carboncoated natural graphite as a lithium-ion battery anode material. Journal of The Electrochemical Society, 149(4), A499-A503.
36. Nakagawa, H., Domi, Y., Doi, T., Ochida, M., Tsubouchi, S., Yamanaka, T., & Ogumi, Z. (2013). In situ Raman study on the structural degradation of a graphite composite negative-electrode and the influence of the salt in the electrolyte solution. Journal ofPower Sources, 236, 138-144.
37. Fujimoto, H., Tokumitsu, K., Mabuchi, A., Chinnasamy, N., & Kasuh, T. (2010). The anode performance of the hard carbon for the lithium ion battery derived from the oxygen-containing aromatic precursors. Journal of Power Sources, 195(21), 7452-7456.

38. Yang, J., Zhou, X. Y., Li, J., Zou, Y. L., & Tang, J. J. (2012). Study of nano-porous hard carbons as anode materials for lithium ion batteries. Materials Chemistry and Physics, 135(2-3), 445-450.
39. Bridges, C. A. , Sun, X. G., Zhao, J., Paranthaman, M. P., & Dai, S. (2012). In situ observation of solid electrolyte interphase formation in ordered mesoporous hard carbon by small-angle neutron scattering. The Journal of Physical Chemistry c, 11604), 7701-7711.
40. Yu, Y., cui, C., Qian, W., Xie, Q., Zheng, C., Kong, C., & Wei, F. (2013). Carbon nanotube production and application in energy storage. Asia-Pacific Journal of Chemical Engineering, 8(2), 234-245.
41. Liang, M., & Zhi, L. (2009). Graphene-based electrode materials for rechargeable lithium batteries. Journal ofMaterials Chemistry, /9(33), 5871-5878.
42. Moretti, A., Kim, G. T., Bresser, Renger, K., Paillard, E., Marassi, R., & Passerini, S. (2013). Investigation of different binding agents for nanocrystalline anatase TiO2 anodes and its application in a novel, green lithium-ion battery. Journal ofPower Sources, 221, 419-426.
43. Wu, F., Wang, Z., Li, X., Guo, H., Yue, P., Xiong, X., & Z.han Q. (2012). Characterization of spherical-shaped Li4Ti5012 prepared by spray drying. Electrochimica Acta, 78, 331-339
44. J. Yuan, X. Liu, H. Zhang, Lithium-ion batteries: advanced materials andtechnologies, CRC Press, 2011.
45. A. Eftekhari, J. Power Sources, 343 (2017) 395-41 1
46. C. Gong, Z. xue, S. wen, Y. Ye, X. Xie, J. Power Sources, 318 (2016) 93-1 12.
47. J. Xu, G. Chen, Physica B: Condensed Matter, 405 (2010) 803-807.
48. O. Toprakci, H.A. Toprakci, L. Ji, X. Zhang, Chemlnform, 42 (2011).
49. J. Xu, G. Chen, Physica B: Condensed Matter, 405 (2010) 803-807.
50. W.-J. Zhang, J. Power Sources, 196 (2011) 2962-2970.

51. Y. Zhang, Q.-y. Huo, P.-p. Du, L.-z. Wang, A.-q. Zhang, Y.-h. Song, Y. Lv, G.-y. Li, Synthetic Metals, 162 (2012) 1315-1326

52. A. Yamada, M. Hosoya, S.-C. Chung, Y. Kudo, K. Hinokuma, K.-Y. Liu, Y. Nishi, J. Power Sources, 1 19 (2003) 232-238

53. F. Zhou, M. Cococcioni, C.A. Marianetti, D. Morgan, G. Ceder, Physical Review B, 70 (2004) 235121.

54. A.K. Padhi, K. Nanjundaswamy, J. Goodenough, J. Electrochem. Soc., 144 (1997) 1188-1194

55. Saroha, R., Panwar, A. K., & Sharma, Y. (2017). Physicochemical and electrochemical performance of LiFe1− xNixPO4 (0≤ x≤ 1.0) solid solution as potential cathode material for rechargeable lithium-ion battery. Ceramics International, 43(7), 5734-5742

56. D.P. Abraham, S. Kawauchi, and D.W. Dees, "Modeling the impedance versus voltage characteristics of LiNi0.08Co0.15Al0.05O2," Electrochim. Acta, vol. 53, pp. 2121–2129, 2008

57. Thi Hang, La.. Enhancement of li–ion battery capacity using nickel doped lifepo4 as cathode material. Vietnam Journal of Science and Technology. 55. 276. 10.15625/2525-2518/55/1B/12119.

58. Rosaiah, P & Padarti, Jeevan & Karanam, Jayanth & Hussain, Owais. (2013). Electrical and electrochemical properties of nanocrystalline LiFePO4 cathode. Applied Physics A. 113. 10.1007/s00339-013-7762-8.

59. M. Schönleber*, C. Uhlmann, P. Braun, A. Weber, E. Ivers-Tiffée .A Consistent Derivation of the Impedance of a Lithium-Ion Battery Electrode and its Dependency on the State-of-Charge , Electrochimica Acta, 4.2017.

60. Y.-J. Lv, J. Su, Y.-F. Long, X.-R. Cui, X.-Y. Lv, Y.-X. Wen, Effects of ball-to-powder weight ratio on the performance of LiFePO4/C prepared by wet-milling assisted carbothermal reduction, Powder Technol. 253 (2014) 467–473.

61. L. Dimesso, C. Spanheimer, W. Jaegermann, Investigation on graphitic carbon foams–LiNiyPO4 (y=0.8–1.0) composites, Solid State Sci. 14 (2012) 1372–1377.
62. J.P. Meyers, M. Doyle, R.M. Darling, J. Newman, The Impedance Response of a Porous Electrode Composed of Intercalation Particles, J. Electrochem. Soc. 147 (2000) 2930.
63. H. Schichlein, A. Müller, M. Voigts, A. Krügel, E. Ivers-Tiffée, Deconvolution of electrochemical impedance spectra for the identification of electrode reaction mechanisms in solid oxide fuel cells, J. Appl. Electrochem. 32 (2002) 875–882,
64. Mayneord, W. V. (1979). "John Alfred Valentine Butler, 14 February 1899 - 16 July 1977". Biographical Memoirs of Fellows of the Royal Society.
65. Alavi, S.M.M.; Birkl, C.R.; Howey, D.A. Time-domain fitting of battery electrochemical impedance models. J. Power Sources 2015, 288, 345–352
66. Temperature dependence of double layer capacitance in lithium-ion battery , Sazzad Hossain Ahmed, S. O. Bade Shrestha, Proceedings of 116th The IIER International Conference, Phuket, Thailand, 9th-10th August 2017
67. Shalini Rodriguesa, N. Munichandraiaha, A. K. Shukla, “AC impedance and state-of-charge analysis of a sealed lithium-ion rechargeable battery”, J Solid State Electrochem (1999).
68. Dai, Haifeng, Bo Jiang, and Xuezhe Wei. "Impedance characterization and modeling of lithium-ion batteries considering the internal temperature gradient." Energies 11.1 (2018): 220
69. Nyquist, Harry (January 1932). "Regeneration Theory". Bell System Technical Journal. USA: American Telephone and Telegraph Company (AT&T). 11 (1): 126–147
70. Dai, Haifeng, Bo Jiang, and Xuezhe Wei. "Impedance characterization and modeling of lithium-ion batteries considering the internal temperature gradient." Energies 11.1 (2018): 220.

71. Electrochemical Impedance: Analysis and Interpretation, J.R. Scully, D.C. Silverman, and M.W. Kendig, editors, ASTM, 1993.

72. J. Newman, K.E. Thomas-Alyea, Electrochemical Systems, John Wiley & Sons, 2004.

73. Electrochemical Methods: Fundamentals and Applications,Allen J. Bard, Larry R. Faulkner,Wiley, ISBN 0471043729, Pg 2

74. Electrochemical Methods: Fundamentals and Applications,Allen J. Bard, Larry R. Faulkner,Wiley, ISBN 0471043729, Pg 102

75. Electrochemical Methods: Fundamentals and Applications,Allen J. Bard, Larry R. Faulkner,Wiley, ISBN 0471043729, Pg 440-445